High-performance photocurrent generation from two-dimensional WS_2 field-effect transistors

Seung Hwan Lee,[1,2,a)] Daeyeong Lee,[1,2,a)] Wan Sik Hwang,[3,b)] Euyheon Hwang,[1] Debdeep Jena,[4] and Won Jong Yoo[1,2,b)]

[1]*Department of Nano Science and Technology, SKKU Advanced Institute of Nano-Technology (SAINT), Sungkyunkwan University (SKKU), 2066 Seobu-ro, Suwon-si, Gyeonggi-do 440-746, South Korea*
[2]*Samsung-SKKU Graphene Center (SSGC), 2066 Seobu-ro, Jangan-gu, Suwon-si, Gyeonggi-do 440-746, South Korea*
[3]*Department of Materials Engineering, Korea Aerospace University, 76 Hanggongdaehang-ro, Deogyang-gu, Goyang-si, Gyeonggi-do 412-791, South Korea*
[4]*Department of Electrical Engineering, University of Notre Dame, Notre Dame, Indiana 46556, USA*

(Received 10 April 2014; accepted 5 May 2014; published online 15 May 2014)

The generation of a photocurrent from two-dimensional tungsten disulfide (WS_2) field-effect transistors is examined here, and its dependence on the photon energy is characterized. We found from the WS_2 devices that a significant enhancement in the ratio of illuminated current against dark current (I_{illum}/I_{dark}) of $\sim 10^2$–10^3 is attained, even with the application of electric fields of $E_D = 0.02$ and $E_G = -22$ mV/nm, which are much smaller than that of the bulk MoS_2 phototransistor. Most importantly, we demonstrate that our multilayer WS_2 shows an extremely high external quantum efficiency of ~7000%, even with the smallest electrical field applied. We also found that photons with an energy near the direct band gap of the bulk WS_2, in the range of 1.9–2.34 eV, give rise to a photoresponsivity of ~0.27 A/W, which exceeds the photoresponsivity of the bulk MoS_2 phototransistor. The superior photosensing properties of WS_2 demonstrated in this work are expected to be utilized in the development of future high performance two-dimensional optoelectronic devices. © *2014 AIP Publishing LLC*. [http://dx.doi.org/10.1063/1.4878335]

Two-dimensional (2D) materials are attractive for use in a variety of electronic devices that can benefit from their atomically thin flexible and transparent layer structures and their low-dimensionality, which provides quantum mechanical properties that are not present in conventional three-dimensional materials.[1,2] 2D materials can potentially enable the devices of the post-silicon era by overcoming the major obstacles presented by current silicon semiconductor devices, including short-channel effects and poor power dissipation. Such materials open avenues for photonic applications that take advantage of variations in a material's band gap properties as a function of the 2D layer thickness.[3]

Transition metal dichalcogenides (TMDC) are the most widely studied 2D materials because they can provide a range of material properties: superconducting, semiconducting, or metallic, depending on the atomic and electronic structures arising from combinations of the transition metal and chalcogen atoms.[3] Particularly, TMDCs formed by Mo or W transition metal atoms can form semiconductors with band gaps that correspond to the visible to infrared absorption spectra.[3] These materials are potentially useful in digital electronics or photonic devices.[4] Recent studies have demonstrated that the band gap of 1.1–2.1 eV (Ref. 3) in a TMDC material is useful for a variety of devices, including photodetectors,[5,6] photovoltaics,[7] light-emitting diodes (LEDs),[8] field-effect transistors (FETs),[9] logic,[10] memory,[11] and sensors.[12]

The TMDC tungsten disulfide (WS_2) has an indirect band gap of 1.4 eV in bulk[13] and a direct band gap of 2.1 eV in a monolayer,[14] which is affected by quantum confinement effects.[15] Although the chemical and atomic structures of WS_2 are similar to those of molybdenum disulfide (MoS_2), WS_2 has been studied to a lesser degree than MoS_2, possibly due to the difficulty in obtaining high quality single crystal WS_2. However, the inert, non-toxic, and environmentally friendly properties of WS_2 make it attractive as a potential electronic material.[1] Field-effect transistors prepared from WS_2 have recently been demonstrated in the previous reports[1,16] and the ambipolar charge carrier characteristic of WS_2,[16–18] which is more frequently reported than other TMDC materials,[19,20] makes it more attractive for use in device applications that involve homogenous or heterogeneous p-n junction. Most importantly, according to the simulation results, WS_2 is reported to have much smaller effective electron mass and to provide better transistor performance than Si as well as MoS_2.[14] The structural, electronic, and optical properties of WS_2 have been studied theoretically[21,22] and experimentally.[23,24] The differential reflectance and photoluminescence (PL) spectra revealed indirect-to-direct gap transition features of WS_2 that resemble those observed in other TMDCs.[25] A Raman spectroscopy study verified that the number of layers in a WS_2 sample could be determined by analyzing the Raman peak shift.[24] Previous studies have described the photosensing properties of TMDC materials, e.g., MoS_2,[26,27] WS_2,[28,29] MoS_2-graphene,[30,31] and MoS_2-silicon[32] heterostructures. Interestingly, investigations into the photoresponse of WS_2, including the spectral photoresponse, the I_{illum}/I_{dark}, and the switching behavior, are rare[29] compared to those that have investigated MoS_2.

In this Letter, we investigate the spectral photoresponse of WS_2, by using an electrical measurement system capable

[a)]S. H. Lee and D. Lee contributed equally to this work.
[b)]Authors to whom correspondence should be addressed. Electronic addresses: whwang@kau.ac.kr and yoowj@skku.edu

of monochromatic light illumination onto a WS_2 field-effect transistor. The optoelectronic properties as the key figures of merit for optical sensors and switching devices, the I_{illum}/I_{dark}, photoresponsivity, and external quantum efficiency (EQE), were measured from WS_2 devices. The spectral response of the external quantum efficiency reveals that an enhanced photocurrent is generated upon illumination at photon energies very close to the direct band gap of WS_2.

A ~20 nm thick multi-layer WS_2 film is mechanically exfoliated from a bulk WS_2 crystal and transferred to a silicon wafer covered by a 90 nm thick silicon dioxide (SiO_2) layer formed on a highly doped *n*-type Si wafer with a resistivity $<5 \times 10^{-3}$ Ω·cm using the conventional micro-mechanical cleavage method.[2] The substrate is baked on a hot plate at 100 °C for 10 min prior to transferring the WS_2 layer and evaporating water molecules onto the surface of the substrate. The thickness of the WS_2 flake is measured using atomic force microscopy (AFM). An AFM image is shown in the right inset of Fig. 1(a). The yellow line is the profile across the path traced by the green line, and the measured thickness of exfoliated WS_2 was ~20 nm (see the yellow arrow).

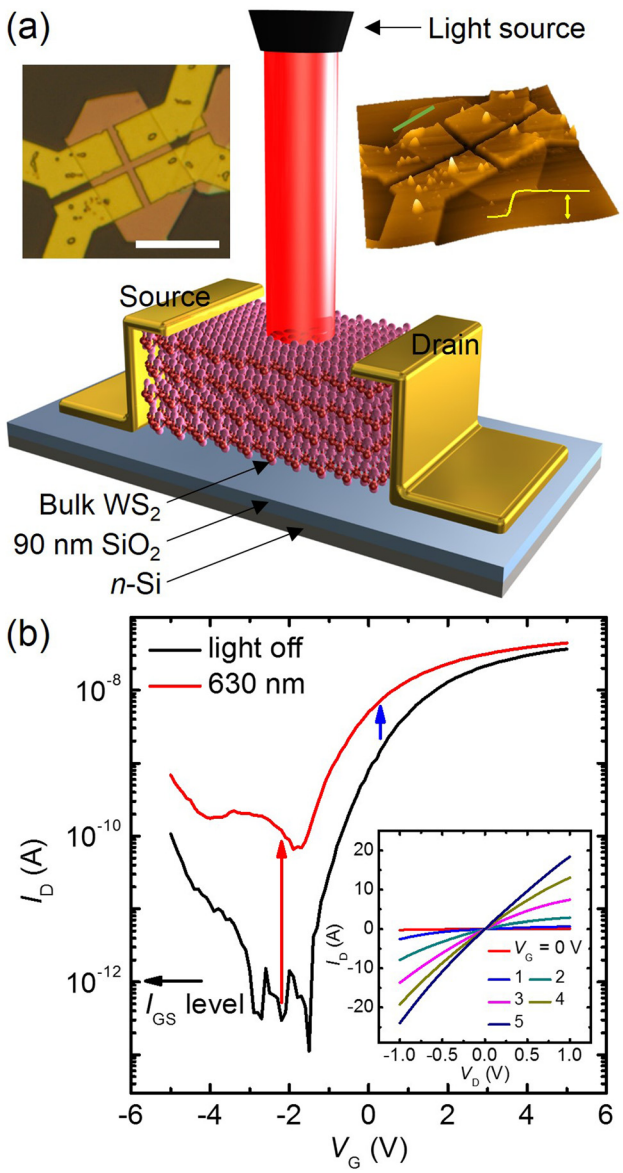

FIG. 1. (a) Schematic diagram showing the WS_2 device and the measurement setup. Right inset: AFM image of a WS_2 device. The yellow line indicates the profile along the green line. Left inset: optical microscope image of the device. Scale bar is 10 μm. (b) Transfer curves with and without light illumination. The I_{illum}/I_{dark} over almost two orders of magnitude is observed near $V_G = -2$ V. The gate leakage level is indicated as a black arrow. Measurements were performed at $V_D = 20$ mV and $P_{opt} = 250$ mW/cm^2. Inset: output curves of the WS_2 device. It shows Ohmic contact behavior.

Field-effect transistor devices are fabricated by patterning and forming source and drain electrodes on the exfoliated WS_2 layer using electron-beam lithography and electron-beam deposition, respectively. The Ti/Au (5/100 nm) is used as the electrodes to form metallic contacts with the WS_2. The highly *n*-doped silicon substrate acts as an electrical back gate to control the charge carriers. Schematic and optical microscope images of the WS_2 device structure are shown in Fig. 1(a) and its left inset, respectively. The electrical and photoresponsivity measurements are conducted under ambient air conditions using a semiconductor parameter analyzer connected to an electrical probe station with a monochromator (see Fig. S2 for the detail structure of the photoresponse measurement system setup[33]).

The FETs of which channels are a bulk WS_2 is fabricated and photoresponse measurement is conducted. The optical microscope and AFM images of the fabricated multi-layer WS_2 phototransistor are shown in left and right insets of Fig. 1(a), respectively. The metal contact of the WS_2 devices forms Ohmic contact, which gives rise to linear output curves (see the inset of Fig. 1(b)). Photo-illumination increases the drain current due to photocurrent generation (see Fig. 1(b)). An I_{illum}/I_{dark} of ~10^2, as estimated by dividing the drain current under photo-illumination by the drain current without photo-illumination, was obtained under a transistor-off gate bias region (see the red arrow in Fig. 1(b)). The I_{illum}/I_{dark} measured under a transistor-on gate bias region is smaller (see the blue arrow in Fig. 1(b)); however, the photocurrent is higher in the positive gate bias region than under a negative gate bias (see Fig. S1[33]) because electrons and holes excited by the incident photons are collected more rapidly under a positive gate bias due to higher carrier velocity in transistor-on gate bias region.

The I_{illum}/I_{dark} and photocurrent density are obtained under various wavelengths of monochromatic light (see Fig. 2). The I_{illum}/I_{dark} increases linearly at illumination power density exceeding ~10 mW/cm^2, whereas the photocurrent increases with the relationship of $J_{ph} = P_{opt}{}^{0.7}$ (see the dotted lines in Fig. 2(b)) across all the measurement ranges, where J_{ph} is the photocurrent density and P_{opt} is the optical power density.[33] An I_{illum}/I_{dark} of ~600 was achieved at $V_g = -2.5$ V and $V_d = 0.002$ V (see the inset of Fig. 2(a)). A larger applied drain bias induced a larger photocurrent at a fixed gate bias (see the inset of Fig. 2(b)). The I_{illum}/I_{dark} and photocurrent could be modulated by varying the electrical biases to further enhance the phototransistor performance. The photoresponsivity of the WS_2 device is ~0.27 A/W and it is calculated from the maximum slope of the linearly plotted lines of solid lines shown in Fig. 2(b) (see Fig. S3[33]). The photoresponsivity of WS_2 was larger than that of MoS_2,[6] probably due to the smaller effective mass of WS_2[34] (see the right inset of Fig. 2(b)).

The external quantum efficiency (EQE $\equiv \eta$) is defined as the number of carriers produced per photon or

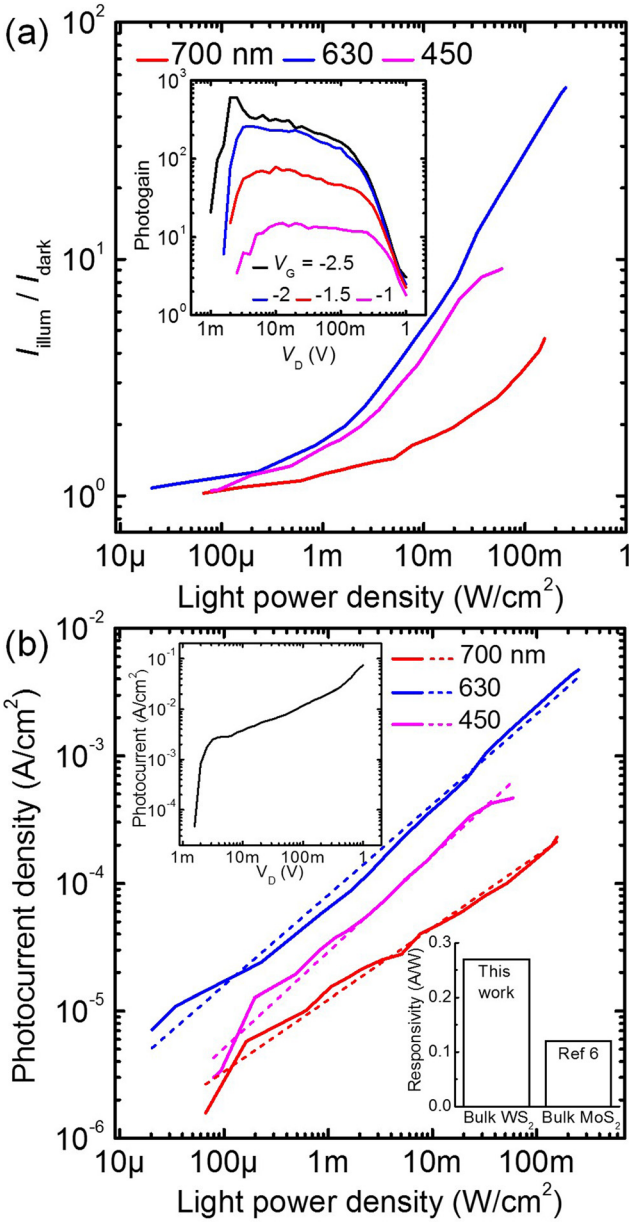

FIG. 2. (a) I_{illum}/I_{dark} as a function of the illumination power density. Measurements were performed at $V_D = 20$ mV and $V_G = -1.5$ V. Inset: Drain and gate bias dependent I_{illum}/I_{dark}. The sample was illuminated at 630 nm and a 250 mW/cm^2 during the measurement. (b) Photocurrent density as a function of the illumination power density. The dotted lines indicate the linear fits to the logarithmically scaled lines. Left inset: Photocurrent as a function of V_D. Measurements were performed at $V_G = -2$ V and $P_{opt} = 250$ mW/cm^2. Right inset: Comparison of the photoresponsivity between the bulk WS_2 and the MoS_2 phototransistors.

$\eta = J_{ph}/(q\phi) = (J_{ph}/q) \times (hv/p_{opt})$, where J_{ph} is the photocurrent density, ϕ is the photon flux ($= P_{opt}/hv$), h is Planck's constant, v is the wavelength of light, q is the electron charge, and P_{opt} is the illumination power density.[35] A high EQE was achieved by modulating the electrical bias applied to the WS_2 device (see Fig. 3(a)). Under a positive gate bias, the EQE is two orders of magnitude greater than the EQE measured under a negative gate bias. The EQE continues to increase as V_D increases. A maximum EQE of ~7000% at a relatively high bias, e.g., $V_D = 1$ V and $V_G = 3$ V, was attained from our measurement, whereas EQE values of ~8% and ~70% are attained at a low V_D of 20 mV for the transistor off-state and on-state, respectively. Our bulk WS_2 phototransistor shows comparable EQE with that of bulk MoS_2 device[6] even ~15-folds smaller application of electric field and three order higher EQE than that of previously reported the phototransistor with multi-layer WS_2 synthesized by chemical vapor deposition[29] (CVD) even with 30-folds smaller application of the electric field (see the inset of Fig. 3(a)). The spectral EQE was measured over the incident wavelength range of 400–700 nm, revealing three peaks (see Fig. 3(b)). The peaks A (~630 nm) and B (~530 nm) originate from the energies of the direct band gaps that formed between the split valance and conduction band at the

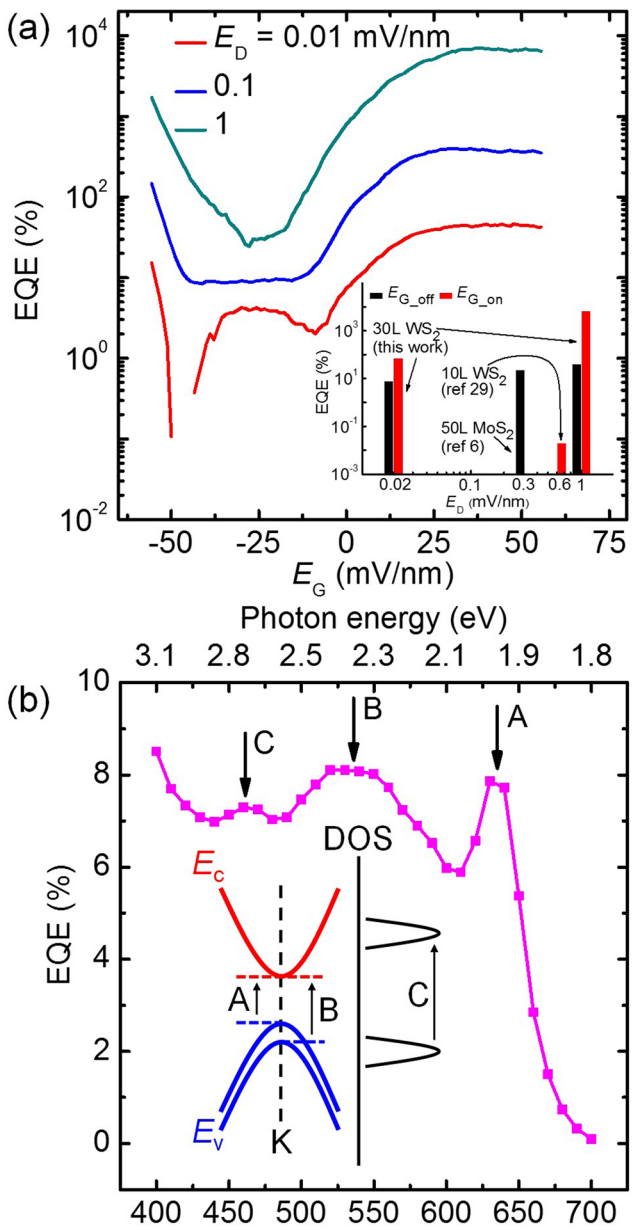

FIG. 3. (a) External quantum efficiency as a function of gate and drain biases, measured at wavelength = 630 nm and $P_{opt} = 250$ mW/cm^2. Inset: Comparison of external quantum efficiency comparison of this work to other reported bulk TMDC phototransistors. E_{G_off} and E_{G_on} in the legend indicate transistor-off and transistor-on gate field, respectively. (b) The spectral external quantum efficiency of WS_2, measured at $V_G = -2.3$ V, $V_D = 20$ mV, and $P_{opt} = 250$ mW/cm^2. The peak positions A, B, and C are related to the electronic structure of the bulk WS_2. Inset: The A, B, and C excitations are described by the schematic diagram of the electronic structure of WS_2.

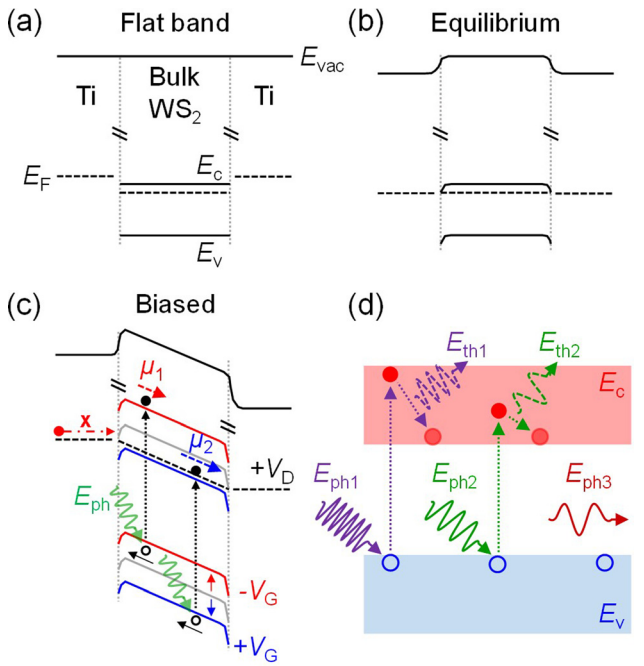

FIG. 4. Band diagrams of a WS_2 device. (a) Flat band state. (b) Equilibrium state: an Ohmic junction is formed. (c) Biased state: the photocurrent generation mechanism depending on gate bias polarity and light illumination is depicted. (d) A schematic drawing of the photocurrent generation dependent on photon energy.

K point of WS_2.[36] Peak C (~460 nm) arises from the optical transition between the density of states peaks in the valence band and the conduction bands[25] (see the inset of Fig. 3). This observation agrees well with a previously reported PL study of WS_2.[25]

Figs. 4(a) and 4(b) show the flat band and equilibrium states of the band diagrams of WS_2 devices, in which the work function of Ti, the band gap of WS_2, and the electron affinity of WS_2 are 4.3, 1.3, and 4.5 eV, respectively.[15] The positive drain bias bends the band structure, as shown in Fig. 4(c). The application of a negative gate bias blocks the charge carrier flow (as indicated by the red dashed-dotted arrow) due to upshifted conduction and valence bands (as indicated by the red line); however, incident photons generate excitons of which separation by the drain bias gives rise to a photocurrent. The application of a positive gate bias increases the charge carrier density by downshifting conduction and valence bands (as indicated by the blue line) and induces a relatively high transconductance in WS_2, which results in higher mobility (as indicated by the blue dotted arrow). The high mobility in the WS_2 channel promotes the collection of excited electrons and yields a higher photocurrent than is obtained under a negative gate bias (as indicated by the red dotted arrow). The photocurrent generated upon illumination increases as the wavelength is changed from 700 nm, 450 nm to 630 nm (see Fig. 2(b)). The 630 nm photons had an energy of 2.07 eV, and this value is close to the direct band gaps of bulk WS_2 (1.98 and 2.25 eV).[37,38] An incident photon with an energy comparable to the direct band gap of WS_2 (as indicated by the green arrow in Fig. 4(d)) is efficiently absorbed with a low energy loss relative to photons having a larger energy (as indicated by the purple arrow in Fig. 4(d)). Such photons generate electron–hole (e-h) pairs that give rise to a large photocurrent. The incident photons with an energy less than the direct band gap of WS_2 are transmitted without generating excitons (see the red arrow in Fig. 4(d)). In this work, we assumed that the photocurrent from a photothermoelectric effect[39] is little altered. The photocurrent generated near source-channel and drain-channel interfaces is canceled each other because the temperature differences between two interfaces are expected to be similar due to global light illumination.[40]

We found a linear photoresponsivity from the WS_2 devices, for illumination powers in the range of 10^{-5}–10^{-1} W/cm^2 and for wavelengths in the range of 450 (2.76)–700 nm (1.77 eV). We demonstrated very high optoelectronic performances from the WS_2 devices: a photoresponsivity of 0.27 A/W, an I_{illum}/I_{dark} of 10^2–10^3, and an external quantum efficiency of ~7000% which are higher than the corresponding values reported for bulk MoS_2 phototransistors and the other reported TMDC photosensing devices, even upon application of the much smaller electrical fields (see Table SI for the detailed comparison[33]).

This work was supported by the Basic Science Research Program through the National Research Foundation of Korea (NRF) (Nos. 2009-0083540 and 2013-015516), and by the Global Frontier R&D Program (No. 2013-073298) on Center for Hybrid Interface Materials (HIM), funded by the Ministry of Science, ICT & Future Planning.

[1]T. Georgiou, R. Jalil, B. D. Belle, L. Britnell, R. V. Gorbachev, S. V. Morozov, Y.-J. Kim, A. Gholinia, S. J. Haigh, O. Makarovsky, L. Eaves, L. A. Ponomarenko, A. K. Geim, K. S. Novoselov, and A. Mishchenko, Nat. Nanotechnol. **8**, 100 (2013).
[2]K. S. Novoselov, A. K. Geim, S. V. Morozov, D. Jiang, Y. Zhang, S. V. Dubonos, I. V. Grigorieva, and A. A. Firsov, Science **306**, 666 (2004).
[3]Q. H. Wang, K. Kalantar-Zadeh, A. Kis, J. N. Coleman, and M. S. Strano, Nat. Nanotechnol. **7**, 699 (2012).
[4]D. Jariwala, V. K. Sangwan, L. J. Lauhon, T. J. Marks, and M. C. Hersam, ACS Nano **8**, 1102 (2014).
[5]H.-M. Li, D.-Y. Lee, M. S. Choi, D. Qu, X. Liu, C.-H. Ra, and W. J. Yoo, Sci. Rep. **4**, 4041 (2014).
[6]W. Choi, M. Y. Cho, A. Konar, J. H. Lee, G.-B. Cha, S. C. Hong, S. Kim, J. Kim, D. Jena, J. Joo, and S. Kim, Adv. Mater. **24**, 5832 (2012).
[7]M. Bernardi, M. Palummo, and J. C. Grossman, Nano Lett. **13**, 3664 (2013).
[8]R. S. Sundaram, M. Engel, A. Lombardo, R. Krupke, A. C. Ferrari, P. Avouris, and M. Steiner, Nano Lett. **13**, 1416 (2013).
[9]S. Das, H.-Y. Chen, A. V. Penumatcha, and J. Appenzeller, Nano Lett. **13**, 100 (2013).
[10]J.-K. Huang, J. Pu, C.-L. Hsu, M.-H. Chiu, Z.-Y. Juang, Y.-H. Chang, W.-H. Chang, Y. Iwasa, T. Takenobu, and L.-J. Li, ACS Nano **8**, 923 (2014).
[11]M. S. Choi, G.-H. Lee, Y.-J. Yu, D.-Y. Lee, S. H. Lee, P. Kim, J. Hone, and W. J. Yoo, Nat. Commun. **4**, 1624 (2013).
[12]D. J. Late, Y.-K. Huang, B. Liu, J. Acharya, S. N. Shirodkar, L. Jiajun, Y. Aiming, D. Charles, U. V. Waghmare, V. P. Dravid, and C. N. R. Rao, ACS Nano **7**, 4879 (2013).
[13]K. K. Kam and B. A. Parkinson, J. Phys. Chem. **86**, 463 (1982).
[14]L. Liu, S. B. Kumar, Y. Ouyang, and J. Guo, IEEE Trans. Electron Devices **58**, 3042 (2011).
[15]A. Kuc, N. Zibouche, and T. Heine, Phys. Rev. B **83**, 245213 (2011).
[16]W. S. Hwang, M. Remskar, R. Yan, V. Protasenko, K. Tahy, S. D. Chae, P. Zhao, A. Konar, H. (Grace) Xing, A. Seabaugh, D. Jena, and W. Hwang, Appl. Phys. Lett. **101**, 013107 (2012).
[17]D. Braga, I. G. Lezama, H. Berger, and A. F. Morpurgo, Nano Lett. **12**, 5218 (2012).
[18]Y. Zhang, Y. Zhang, Q. Ji, J. Ju, H. Yuan, J. Shi, T. Gao, D. Ma, M. Liu, Y. Chen, X. Song, H. Y. Hwang, Y. Cui, and Z. Liu, ACS Nano **7**, 8963 (2013).

[19]Y. Zhang, J. Ye, Y. Matsuhashi, and Y. Iwasa, Nano Lett. **12**, 1136 (2012).
[20]M. M. Perera, M.-W. Lin, H.-J. Chuang, B. P. Chamlagain, C. Wang, X. Tan, M. M.-C. Cheng, D. Tománek, and Z. Zhou, ACS Nano **7**, 4449 (2013).
[21]W. J. Schutte, J. L. De Boer, and F. Jellinek, J. Solid State Chem. **70**, 207 (1987).
[22]J. A. Wilson and A. D. Yoffe, Adv. Phys. **18**, 193 (1969).
[23]W. Zhao, R. M. Ribeiro, M. Toh, A. Carvalho, C. Kloc, A. H. Castro Neto, and G. Eda, Nano Lett. **13**, 5627 (2013).
[24]A. Berkdemir, H. R. Gutiérrez, A. R. Botello-Méndez, N. Perea-López, A. L. Elías, C.-I. Chia, B. Wang, V. H. Crespi, F. López-Urías, J.-C. Charlier, H. Terrones, and M. Terrones, Sci. Rep. **3**, 1755 (2013).
[25]W. Zhao, Z. Ghorannevis, L. Chu, M. Toh, C. Kloc, P.-H. Tan, and G. Eda, ACS Nano **7**, 791 (2013).
[26]D.-S. Tsai, K.-K. Liu, D.-H. Lien, M.-L. Tsai, C.-F. Kang, C.-A. Lin, L.-J. Li, and J.-H. He, ACS Nano **7**, 3905 (2013).
[27]O. Lopez-Sanchez, D. Lembke, M. Kayci, A. Radenovic, and A. Kis, Nat. Nanotechnol. **8**, 497 (2013).
[28]C. Zhang, S. Wang, L. Yang, Y. Liu, T. Xu, Z. Ning, A. Zak, Z. Zhang, R. Tenne, and Q. Chen, Appl. Phys. Lett. **100**, 243101 (2012).
[29]N. Perea-López, A. L. Elías, A. Berkdemir, A. Castro-Beltran, H. R. Gutiérrez, S. Feng, R. Lv, T. Hayashi, F. López-Urías, S. Ghosh, B. Muchharla, S. Talapatra, H. Terrones, and M. Terrones, Adv. Funct. Mater. **23**, 5511 (2013).
[30]W. Zhang, C.-P. Chuu, J.-K. Huang, C.-H. Chen, M.-L. Tsai, Y.-H. Chang, C.-T. Liang, Y.-Z. Chen, Y.-L. Chueh, J.-H. He, M.-Y. Chou, and L.-J. Li, Sci. Rep. **4**, 3826 (2014).
[31]W. J. Yu, Y. Liu, H. Zhou, A. Yin, Z. Li, Y. Huang, and X. Duan, Nat. Nanotechnol. **8**, 952 (2013).
[32]M. R. Esmaeili-Rad and S. Salahuddin, Sci. Rep. **3**, 2345 (2013).
[33]See supplementary material at http://dx.doi.org/10.1063/1.4878335 for gate bias and wavelength dependent transfer curve and photocurrent, photoresponse measurement system setup, calculation of photocurrent density and optical power density, comparison of the figures of merit for photodetectors prepared using different TMDCs, and photoresponsivity calculation.
[34]H. Shi, H. Pan, Y.-W. Zhang, and B. I. Yakobson, Phys. Rev. B **87**, 155304 (2013).
[35]S. M. Sze and K. K. Ng, *Physics of Semiconductor Devices*, 3rd ed. (John Wiley & Sons, Inc., Hoboken, 2007).
[36]R. Winkler, *Spin-Orbit Coupling Effects in Two-Dimensional Electron and Hole Systems* (Springer, Berlin, Heidelberg, Germany, 2003), p. 228.
[37]A. R. Beal, J. C. Knights, and W. Y. Liang, J. Phys. C **5**, 3540 (1972).
[38]R. A. Bromley, R. B. Murray, and A. D. Yoffe, J. Phys. C **5**, 759 (1972).
[39]M. Buscema, M. Barkelid, V. Zwiller, H. S. J. van der Zant, G. A. Steele, and A. Castellanos-Gomez, Nano Lett. **13**, 358 (2013).
[40]N. Perea-López, Z. Lin, N. R. Pradhan, A. Iñiguez-Rábago, A. L. Elías, A. McCreary, J. Lou, P. M. Ajayan, H. Terrones, L. Balicas, and M. Terrones, 2D Mater. **1**, 011004 (2014).